Available online at www.sciencedirect.com
SCIENCE DIRECT®
PERGAMON
International Journal of Heat and Mass Transfer 46 (2003) 5031–5044
International Journal of HEAT and MASS TRANSFER
www.elsevier.com/locate/ijhmt

Non-thermal equilibrium melting of granular packed bed in horizontal forced convection. Part II: numerical simulation

Y.L. Hao, Y.-X. Tao *

Department of Mechanical and Materials Engineering, Florida International University, Miami, FL 33199, USA

Received 6 March 2003; received in revised form 2 July 2003

Abstract

A mathematic model based on the theory of interacting continua is developed to describe the complex liquid–solid two-phase flow with phase-change particles as encountered in non-thermal equilibrium melting of granular packed bed subject to horizontal, forced convection. The model is solved numerically using the SIMPLE method, in which the pressure correction based on two-phase mixture continuity equation is implemented. Conservation equations are solved in the entire computational domain including both the liquid–solid region and liquid-only region. It is ensured that the global mass, momentum, and energy of two phases are conserved. The local volume-averaged solid velocity and solid volume fractions are predicted as variables so that the moving and repacking of solid particles can be simulated. This is a step forward from the results published in the open literature where the assumptions of zero-relative motion of solid particles and constant porosity or the constant volume are often used. In addition, the model provides the detailed information about the motion of two phases and phase-change characteristics. Within the uncertainty, the simulation results agree reasonably with the available experimental data presented in Part I of this study [1].

Keywords: Numerical simulation; Mathematical model; Packed bed; Phase change; Convective heat transfer

1. Introduction

The melting phenomena of dispersed or packed solid particles in a fluid has been of interest in recent years since the understanding of the process is very important for the safety of space applications and the need for an increased number of applications in material processing. Kearns and Plumb [2] studied experimentally the contact melting of a packed bed. Plumb [3] presented a numerical analysis of convective melting of packed beds. In his analysis, thermal non-equilibrium is considered, but the granular motion is neglected. The very limited motion of the particles was allowed in a later work [4]. They adopted the constant porosity model and the constant volume model to prescribe the motion process of the packed bed. Sabau and Tao [5] proposed a model to predict the melting characteristics during one- and two-dimensional convective melting processes for a packed bed. Jiang et al. [6] developed a numerical modeling of two-dimensional convective melting of granular packed beds based on Sabau and Tao's work [5]. They divided the entire computational domain into two sub-domains, the pure fluid and the melting packed bed. The single-phase model and two-phase model was used for two sub-domains, respectively.

In the present paper, we focus on the development of a three-dimensional numerical technique that allows the simulation of the forced convective melting of a packed bed subject to a horizontal fluid flow of the same species. To the best of our knowledge, this is the first numerical study that addresses this issue.

We choose a finite-difference scheme based on the SIMPLE method [7] to simulate the complex liquid–solid two-phase flow with phase change as encountered

* Corresponding author. Tel.: +1-305-348-3015; fax: +1-305-348-1932.
E-mail address: taoy@fiu.edu (Y.-X. Tao).

0017-9310/$ - see front matter © 2003 Elsevier Ltd. All rights reserved.
doi:10.1016/S0017-9310(03)00360-0

Nomenclature

a	coefficient in the discretization equation
c_p	specific heat at constant pressure [J/(kg K)]
D	virtual mass coefficient
d_p	particle diameter [m]
G	particle–particle interaction modulus [Pa]
$\mathbf{g}$	gravitational acceleration vector [m/s^2]
h	volumetric heat transfer coefficient [W/(m^3 K)]
h_{ls}	latent heat for fusion [J/kg]
h_p	heat transfer coefficient [W/(m^2 K)]
k	thermal conductivity [W/(m K)]
M	mass of packed bed [kg]
$\dot{m}$	mass generation rate [kg/(m^3 s)]
Nu_p	Nusselt number, $h_p d_p/k_l$
Pr	Prandtl number
p	pressure [Pa]
Re_p	Reynolds number, $\varepsilon\rho_l\lvert\mathbf{v}_l-\mathbf{v}_s\rvert d_p/\mu_l$
S	general source term
T	temperature [°C]
T_m	melting temperature [°C]
t	time [s]
u	x-direction velocity [m/s]
$\mathbf{v}$	velocity vector [m/s]
v	y-direction velocity [m/s]
w	z-direction velocity [m/s]
x, y, z	coordinates

Greek symbols

β	friction coefficient [kg/(m^3 s)]
ε	volume fraction
μ	viscosity [Pa s]
ρ	density [kg/m^3]
φ	general dependent variable

Subscripts

eff	effective
I	interface
l	liquid
s	solid
α	phase

Superscripts

0	old value (at time t) of the variable
*	previous-iteration value of a variable

in the convective melting process for a packed bed. It is because the SIMPLE method has achieved the success in the numerical simulation of single-phase fluid flow and heat transfer with relative rigor of clearly defined first-principles. Another reason is that the method can save large amount of computer time and storage. The grid system utilized treats the interface between the liquid–solid region and liquid-only region as internal grids instead of using boundary-fitted coordinates along the interface. All of conservation equations are solved in the entire computational domain, including the liquid–solid two-phase region and the liquid-only region, to ensure the global conservation of mass, momentum and energy of two phases. The motion and volume fraction of solid phase during a melting process are calculated to simulate the movement and repacking phenomenon of solid particles. This approach removes the needs to assume motionless solid particles and the constant porosity or the constant volume, as previously done in other studies [4]. The detailed results such as velocity and temperature profiles of two phases and phase-change characteristics can be obtained.

In this study, turbulence is not considered for two reasons. One is that for the cases studied fluid velocities are relatively low, and the turbulent-dispersion created by "jets" and "wakes" in the interstices is not strong enough to have a significant effect. The other reason is that because volume-averaged equations are used in the formulation, the issue of turbulence cannot be treated explicitly. Therefore, the hydrodynamic model in this study does not contain turbulence terms.

2. Theoretical model

The model of two-phase flow and heat–mass transfer with the phase changes is based on the theory of interacting continua [8]. The interfaces between the fluid and solid particles can be considered as surfaces of discontinuity. Consequently, the balance laws for each phase are expressed in terms of partial differential equations, whereas on the interface they are formulated in terms of jump conditions. In principle, the system of governing equations with the initial and boundary conditions and the jump conditions on the interface can be solved numerically. However, the complexity of the geometry of the interface is for most practical problems sufficiently complex to render this alternative unfeasible. It is therefore desirable to simplify the problem by volume averaging over a representative elementary volume in the two-phase flow. The both phases are treated as continuum media. The complex jump conditions on the interface are transformed to the terms related to the interaction between the two phases in the averaged equations, which can be obtained by using the proper correlations. The local volume-averaged equations of mass, momentum and energy conservation can be expressed by the following with their symbols defined in the nomenclature.

2.1. Governing equations

Continuity

$$\frac{\partial}{\partial t}(\varepsilon_l\rho_l) + \nabla\cdot(\varepsilon_l\rho_l\mathbf{v}_l) = \dot{m}, \tag{1}$$

$$\frac{\partial}{\partial t}(\varepsilon_s\rho_s) + \nabla\cdot(\varepsilon_s\rho_s\mathbf{v}_s) = -\dot{m}. \tag{2}$$

Momentum

$$\begin{aligned}&\frac{\partial}{\partial t}(\varepsilon_l\rho_l\mathbf{v}_l) + \nabla\cdot(\varepsilon_l\rho_l\mathbf{v}_l\mathbf{v}_l)\\ &\quad= -\varepsilon_l\nabla p + \nabla\cdot[\varepsilon_l\mu_l(\nabla\mathbf{v}_l + \nabla\mathbf{v}_l^{\mathrm{T}})] + \varepsilon_l\rho_l\mathbf{g} - \beta(\mathbf{v}_l - \mathbf{v}_s)\\ &\qquad+ (1-\varepsilon_l)D\rho_l\frac{\mathrm{d}}{\mathrm{d}t}(\mathbf{v}_l - \mathbf{v}_s) + \dot{m}\mathbf{v}_l,\end{aligned} \tag{3}$$

$$\begin{aligned}&\frac{\partial}{\partial t}(\varepsilon_s\rho_s\mathbf{v}_s) + \nabla\cdot(\varepsilon_s\rho_s\mathbf{v}_s\mathbf{v}_s)\\ &\quad= -\varepsilon_s\nabla p - G\nabla\varepsilon_l + \nabla\cdot[\varepsilon_s\mu_s(\nabla\mathbf{v}_s + \nabla\mathbf{v}_s^{\mathrm{T}})] + \varepsilon_s\rho_s\mathbf{g}\\ &\qquad+ \beta(\mathbf{v}_l - \mathbf{v}_s) - (1-\varepsilon_l)D\rho_l\frac{\mathrm{d}}{\mathrm{d}t}(\mathbf{v}_l - \mathbf{v}_s) - \dot{m}\mathbf{v}_s.\end{aligned} \tag{4}$$

Thermal energy

$$\frac{\partial}{\partial t}(\varepsilon_l\rho_l i_l) + \nabla\cdot(\varepsilon_l\rho_l i_l\mathbf{v}_l) = \nabla\cdot(\varepsilon_l k_{\mathrm{eff},l}\nabla T_l) - h(T_l - T_s) + \dot{m}i_{\mathrm{l-l}}, \tag{5}$$

$$\begin{aligned}&\frac{\partial}{\partial t}(\varepsilon_s\rho_s i_s) + \nabla\cdot(\varepsilon_s\rho_s i_s\mathbf{v}_s)\\ &\quad= \nabla\cdot(\varepsilon_s k_{\mathrm{eff},s}\nabla T_s) + h(T_l - T_s) - \dot{m}i_{\mathrm{l-s}}.\end{aligned} \tag{6}$$

For a liquid–solid two-phase system, the relationship between liquid and solid volume fraction is $\varepsilon_l + \varepsilon_s = 1$. Therefore, only one of liquid and solid volume fractions is an independent variable. In the thermal energy equations, the pressure terms, the dissipation function terms and the terms of Joule's heating and thermal radiation have been neglected.

For solving the governing equations, the basic variables must be specified. In this study, the basic variables have been chosen as the liquid volume fraction, ε_l, the pressure, p, three components of liquid velocity vector, u_l, v_l, w_l, three components of solid phase velocity vector, u_s, v_s, w_s, the liquid phase enthalpy, i_l, and the solid phase enthalpy, i_s. For the closure of the set of governing equations, specification of the constitutive equations is required. This means that all other variables in the governing equations must be specified in terms of the basic variables.

In this study, the simulation case involves a granular packed bed that is subject to a fluid flow with a temperature higher than the phase-change temperature of the particle material. Therefore, the particles in the packed bed are heated and melt when their surface temperature reaches the phase-change temperature. The melting of solid phase causes the mass transport from solid phase to liquid phase. This phenomenon is represented as a source term on the right hand side of two-phase continuity equations. The momentum and energy transports between two phases caused by the mass transport are presented by the corresponding terms in momentum and energy equations for the liquid and solid, respectively. The model adopted in the present study considers that both phases are continuous and fully interpenetrating. The difference between the temperatures at the surface and at the interior of the particle is not considered for the reason of reducing a significant portion of computing time.

2.2. Constitutive equations

The melting rate of solid phase per unit volume, the source term in the liquid continuity equation, can be calculated using the energy balance relation, which requires that the latent heat of melting be related to heat transfer from the liquid to the solid phase, i.e.,

$$\dot{m} = \begin{cases} 0, & T_s < T_m,\\ \frac{h(T_l - T_s)}{h_{ls}}, & T_s = T_m.\end{cases} \tag{7}$$

The friction coefficient β in Eqs. (3) and (4) is calculated in two ranges of liquid phase volume fraction. If $\varepsilon_l < 0.8$, the friction coefficient β is obtained from Ergun equation as follows [9]:

$$\beta = 150\frac{(1-\varepsilon_l)^2\mu_l}{\varepsilon_l d_p^2} + 1.75\frac{(1-\varepsilon_l)\rho_l}{d_p}|\mathbf{v}_l - \mathbf{v}_s|. \tag{8}$$

If $\varepsilon_l \geqslant 0.8$, the friction coefficient β becomes

$$\beta = \frac{3}{4}C_d\frac{\varepsilon_l(1-\varepsilon_l)}{d_p}\rho_l|\mathbf{v}_l - \mathbf{v}_s|\varepsilon_l^{-2.65}. \tag{9}$$

In this formula, $\varepsilon_l^{-2.65}$ shows the effect due to the presence of other particles in the fluid and acts as a correction to the usual Stokes law for free fall of a single particle [9]. C_d is related to the particle Reynolds number [10]

$$C_d = \begin{cases} \frac{24}{Re_p}(1 + 0.15Re_p^{0.687}), & Re_p < 1000,\\ 0.44, & Re_p \geqslant 1000,\end{cases} \tag{10}$$

where

$$Re_p = \frac{\varepsilon_l\rho_l|\mathbf{v}_l - \mathbf{v}_s|d_p}{\mu_l}. \tag{11}$$

In Eqs. (3) and (4), D is the virtual mass coefficient. For dispersed spherical particles, $D = 0.5$ [11].

The following formula [12] is applied to the particle–particle interaction modulus G in Eq. (4):

$$G = -1.0\mathrm{e}^{100(0.45-\varepsilon_l)}. \tag{12}$$

The viscosity of solid phase μ_s has to be obtained since the solid phase is considered as a continuum in the present model. In fact, due to the lack of experimental study the data of viscosity μ_s have not been available for

the system of liquid–solid two-phase flow with melting solid. As a first-degree approximation, the best simulation using an indirect comparison with melting rate of experimental data is obtained in this study when the value of $\mu_s = 0.01$ Pa s is chosen.

The temperatures of the liquid and solid phases, T_l and T_s, on the right sides in Eqs. (5) and (6) can be calculated from the enthalpy formulations as following,

$$i_l = c_{p,l}T_l + [(c_{p,s} - c_{p,l})T_m + h_{ls}], \tag{13}$$

$$i_s = c_{p,s}T_s. \tag{14}$$

The last terms on the right side in Eqs. (5) and (6) represent the enthalpy transfer between the two phases because of phase change. Since the melting from solid phase enters the liquid phase at the melting temperature, the enthalpy transfer terms in Eqs. (5) and (6) can be expressed as, respectively,

$$\dot{m}i_{l-l} = \dot{m}(c_{p,s}T_m + h_{ls}), \tag{15}$$

$$\dot{m}i_{l-s} = \dot{m}c_{p,s}T_m. \tag{16}$$

The effective thermal conductivities in Eqs. (5) and (6) are calculated using the approximate model in [13]:

$$k_{eff,l} = \left(1 - \sqrt{1-\varepsilon_l}\right)k_l/\varepsilon_l, \tag{17}$$

$$k_{eff,s} = \frac{\sqrt{1-\varepsilon_l}}{1-\varepsilon_l}[\eta A + (1-\eta)Z]k_l, \tag{18}$$

where

$$Z = \frac{2(B - B/A)}{(1-B/A)^3}\ln\left(\frac{A}{B}\right) - \frac{2(B-1)}{(1-B/A)^2} - \frac{B+1}{1-B/A}, \tag{19}$$

and

$$B = 1.25(1/\varepsilon_l - 1)^{10/9}. \tag{20}$$

For spherical particles, $A = k_s/k_l$ and $\eta = 7.26 \times 10^{-3}$.

The volumetric heat transfer coefficient h in Eqs. (5) and (6) is obtained from

$$h = \frac{6(1-\varepsilon_l)}{d_p}h_p. \tag{21}$$

In this formula, the heat transfer coefficient h_p can be estimated according to [14]:

$$Nu_p = \frac{h_p d_p}{k_l} = 2 + 1.1Re_p^{0.6}Pr^{1/3}. \tag{22}$$

The diameter of particle can be estimated based on the relation that the loss of mass particle in the interval Δt equals the melting mass of particle in the same interval Δt. We assume particles retain their sphericity in the melting process, therefore,

$$d_p = d_p^0\left(1 - \frac{\dot{m}\Delta t}{\varepsilon_s\rho_s}\right)^{1/3}. \tag{23}$$

3. Numerical method

The set of 10 non-linear, coupled, partial differential equations presented in Eqs. (1)–(6), supplemented with the constitutive equations and the initial and boundary conditions, cannot be solved analytically. Therefore, a numerical method must be used to obtain an approximate solution. In the present study, we developed a numerical method based on the SIMPLE algorithm [7] to solve the above conservation equations in three-dimensional Cartesian coordinate system.

Eqs. (1)–(6), can be written as a general differential equation:

$$\frac{\partial}{\partial t}(\varepsilon_\alpha\rho_\alpha\varphi_\alpha) + \frac{\partial}{\partial x_j}(\varepsilon_\alpha\rho_\alpha v_{\alpha,j}\varphi_\alpha) = \frac{\partial}{\partial x_j}\left(\varepsilon_\alpha\Gamma_\varphi\frac{\partial\varphi_\alpha}{\partial x_j}\right) + S_\varphi. \tag{24}$$

For the basic variable, an appropriate value is given to the diffusion coefficient Γ_φ and the source term S_φ in Table 1. The source term that is the non-linear function of variable φ_α has to be linearized as $S_\varphi = S_C + S_P\varphi_\alpha$, because the differential equation has to be discretized as the linear algebraic equation in order to be solved by the techniques for linear algebraic equations [7]. The linearization treatments of the source terms are given in Table 1.

We utilize a staggered grid system. The grid point is placed at the geometric center of the control volume. Field variables such as p, ρ, ε and i are grid-centered quantities, whereas velocities are located on the sides of grids, as shown in Fig. 1. Integer indices i, j and k count control-volume centers in the x-, y-, and z-directions, respectively, whereas half integer indices refer to the edge positions of control volume.

3.1. Discretized equations

We integrated the general differential equation over the control volume shown in Fig. 1. The fully implicit scheme was adopted for the time coordinate. The power-law scheme was adopted for the convective and diffusive terms. The above-mentioned set of governing equations written in the general differential equation form is discretized as following general form after rearrangement.

$$a\varphi_{i,j,k} = a_{i+1}\varphi_{i+1} + a_{i-1}\varphi_{i-1} + a_{j+1}\varphi_{j+1} + a_{j-1}\varphi_{j-1} + a_{k+1}\varphi_{k+1} + a_{k-1}\varphi_{k-1} + b, \tag{25}$$

where

$$a_{i+1} = \left\{\frac{(\varepsilon\Gamma)_{i+1/2}}{x_{i+1}-x_i}\left[\left[0,\left(1 - 0.1\left|\frac{x_{i+1}-x_i}{(\varepsilon\Gamma)_{i+1/2}/(\varepsilon\rho u)_{i+1/2}}\right|\right)^5\right]\right] + [[0, -(\varepsilon\rho u)_{i+1/2}]]\right\}\Delta y\Delta z, \tag{26a}$$

Table 1
Relationship between the governing equations and the general differential equation

φ	Γ	Source-term linearization $S = S_C + S_P\varphi$	
		S_C	S_P
ε_l	0	$\dot{m}$	0
u_l	$\varepsilon_l\mu_l$	$\frac{\partial}{\partial x}\left(\varepsilon_l\mu_l\frac{\partial u_l}{\partial x}\right)+\frac{\partial}{\partial y}\left(\varepsilon_l\mu_l\frac{\partial v_l}{\partial x}\right)+\frac{\partial}{\partial z}\left(\varepsilon_l\mu_l\frac{\partial w_l}{\partial x}\right)-\varepsilon_l\frac{\partial p}{\partial x}$ $+\varepsilon_l\rho_l g_x+\beta_x u_s+(1-\varepsilon_l)D\rho_l\frac{d}{dt}(u_l-u_s)+[[\dot{m},0]]u_l$	$-\beta_x-[[-\dot{m},0]]$
v_l	$\varepsilon_l\mu_l$	$\frac{\partial}{\partial x}\left(\varepsilon_l\mu_l\frac{\partial u_l}{\partial y}\right)+\frac{\partial}{\partial y}\left(\varepsilon_l\mu_l\frac{\partial v_l}{\partial y}\right)+\frac{\partial}{\partial z}\left(\varepsilon_l\mu_l\frac{\partial w_l}{\partial y}\right)-\varepsilon_l\frac{\partial p}{\partial y}+\varepsilon_l\rho_l g_y$ $+\beta_y v_s+(1-\varepsilon_l)D\rho_l\frac{d}{dt}(v_l-v_s)+[[\dot{m},0]]v_l$	$-\beta_y-[[-\dot{m},0]]$
w_l	$\varepsilon_l\mu_l$	$\frac{\partial}{\partial x}\left(\varepsilon_l\mu_l\frac{\partial u_l}{\partial z}\right)+\frac{\partial}{\partial y}\left(\varepsilon_l\mu_l\frac{\partial v_l}{\partial z}\right)+\frac{\partial}{\partial z}\left(\varepsilon_l\mu_l\frac{\partial w_l}{\partial z}\right)-\varepsilon_l\frac{\partial p}{\partial z}+\varepsilon_l\rho_l g_z$ $+\beta_z w_s+(1-\varepsilon_l)D\rho_l\frac{d}{dt}(w_l-w_s)+[[\dot{m},0]]w_l$	$-\beta_z-[[-\dot{m},0]]$
i_l	$\frac{\varepsilon_l k_{eff,l}}{c_{p,l}}$	$\frac{h}{c_{p,l}}i_s+\frac{h}{c_{p,s}}[(c_{p,s}-c_{p,l})T_m+h_{ls}]+\dot{m}(c_{p,s}T_m+h_{ls})$	$-\frac{h}{c_{p,l}}$
u_s	$\varepsilon_s\mu_s$	$\frac{\partial}{\partial x}\left(\varepsilon_s\mu_s\frac{\partial u_s}{\partial x}\right)+\frac{\partial}{\partial y}\left(\varepsilon_s\mu_s\frac{\partial v_s}{\partial x}\right)+\frac{\partial}{\partial z}\left(\varepsilon_s\mu_s\frac{\partial w_s}{\partial x}\right)-\varepsilon_s\frac{\partial p}{\partial x}+\varepsilon_s\rho_s g_x$ $+\beta_x u_l-(1-\varepsilon_l)D\rho_l\frac{d}{dt}(u_l-u_s)-G\frac{\partial\varepsilon_l}{\partial x}+[[-\dot{m},0]]u_s$	$-\beta_x-[[\dot{m},0]]$
v_s	$\varepsilon_s\mu_s$	$\frac{\partial}{\partial x}\left(\varepsilon_s\mu_s\frac{\partial u_s}{\partial y}\right)+\frac{\partial}{\partial y}\left(\varepsilon_s\mu_s\frac{\partial v_s}{\partial y}\right)+\frac{\partial}{\partial z}\left(\varepsilon_s\mu_s\frac{\partial w_s}{\partial y}\right)-\varepsilon_s\frac{\partial p}{\partial y}+\varepsilon_s\rho_s g_y$ $+\beta_y v_l-(1-\varepsilon_l)D\rho_l\frac{d}{dt}(v_l-v_s)-G\frac{\partial\varepsilon_l}{\partial y}+[[-\dot{m},0]]v_s$	$-\beta_y-[[\dot{m},0]]$
w_s	$\varepsilon_s\mu_s$	$\frac{\partial}{\partial x}\left(\varepsilon_s\mu_s\frac{\partial u_s}{\partial z}\right)+\frac{\partial}{\partial y}\left(\varepsilon_s\mu_s\frac{\partial v_s}{\partial z}\right)+\frac{\partial}{\partial z}\left(\varepsilon_s\mu_s\frac{\partial w_s}{\partial z}\right)-\varepsilon_s\frac{\partial p}{\partial z}+\varepsilon_s\rho_s g_z$ $+\beta_z w_l-(1-\varepsilon_l)D\rho_l\frac{d}{dt}(w_l-w_s)-G\frac{\partial\varepsilon_l}{\partial z}+[[-\dot{m},0]]w_s$	$-\beta_z-[[\dot{m},0]]$
i_s	$\frac{\varepsilon_s k_{eff,s}}{c_{p,s}}$	$\frac{h}{c_{p,l}}[i_l-(c_{p,s}-c_{p,l})T_m-h_{ls}]-\dot{m}c_{p,s}T_m$	$-\frac{h}{c_{p,s}}$

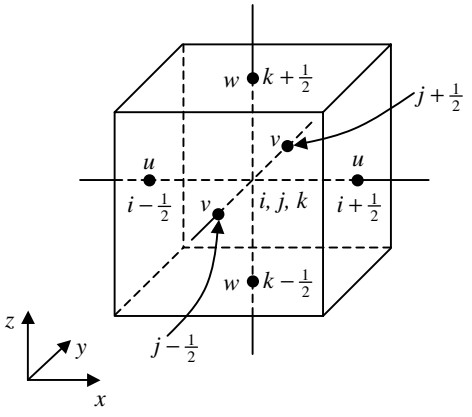

Fig. 1. Layout for a computational grid.

$$a_{i-1}=\left\{\frac{(\varepsilon\Gamma)_{i-1/2}}{x_i-x_{i-1}}\left[\left[0,\left(1-0.1\left|\frac{x_i-x_{i-1}}{(\varepsilon\Gamma)_{i-1/2}/(\varepsilon\rho u)_{i-1/2}}\right|\right)^5\right]\right]+[[0,-(\varepsilon\rho u)_{i-1/2}]]\right\}\Delta y\Delta z, \tag{26b}$$

$$a_{j+1}=\left\{\frac{(\varepsilon\Gamma)_{j+1/2}}{y_{j+1}-y_j}\left[\left[0,\left(1-0.1\left|\frac{y_{j+1}-y_j}{(\varepsilon\Gamma)_{j+1/2}/(\varepsilon\rho v)_{j+1/2}}\right|\right)^5\right]\right]+[[0,-(\varepsilon\rho v)_{j+1/2}]]\right\}\Delta z\Delta x, \tag{26c}$$

$$a_{j-1}=\left\{\frac{(\varepsilon\Gamma)_{j-1/2}}{y_j-y_{j-1}}\left[\left[0,\left(1-0.1\left|\frac{y_j-y_{j-1}}{(\varepsilon\Gamma)_{j-1/2}/(\varepsilon\rho v)_{j-1/2}}\right|\right)^5\right]\right]+[[0,-(\varepsilon\rho v)_{j-1/2}]]\right\}\Delta z\Delta x, \tag{26d}$$

$$a_{k+1}=\left\{\frac{(\varepsilon\Gamma)_{k+1/2}}{z_{k+1}-z_k}\left[\left[0,\left(1-0.1\left|\frac{z_{k+1}-z_k}{(\varepsilon\Gamma)_{k+1/2}/(\varepsilon\rho w)_{k+1/2}}\right|\right)^5\right]\right]+[[0,-(\varepsilon\rho w)_{k+1/2}]]\right\}\Delta x\Delta y, \tag{26e}$$

$$a_{k-1}=\left\{\frac{(\varepsilon\Gamma)_{k-1/2}}{z_k-z_{k-1}}\left[\left[0,\left(1-0.1\left|\frac{z_k-z_{k-1}}{(\varepsilon\Gamma)_{k-1/2}/(\varepsilon\rho w)_{k-1/2}}\right|\right)^5\right]\right]+[[0,-(\varepsilon\rho w)_{k-1/2}]]\right\}\Delta x\Delta y, \tag{26f}$$

$$a=a_{i+1}+a_{i-1}+a_{j+1}+a_{j-1}+a_{k+1}+a_{k-1}+(\rho^0/\Delta t-S_P)\Delta x\Delta y\Delta z, \tag{26g}$$

$$b=(\rho^0\varphi^0/\Delta t+S_C)\Delta x\Delta y\Delta z. \tag{26h}$$

We omitted the subscripts denoting phases and variables in above equations and formulas for simplicity. The discretization equations obtained in this manner present the conservation principles for φ for the finite control volume. The resulting solution would imply that the integral conservation of mass, momentum, and energy is completely satisfied over any group of control volumes and, most importantly, over the whole computational domain. This is true even for a coarse-grid solution, which is very helpful during debugging of the computer code.

3.2. Corrections to velocities and pressure

To utilize the computing resource more efficiently, we employ the iterative method, instead of a direct, simultaneous solution scheme for all governing equations, in order to yield the volume fraction, velocity components, pressure, and enthalpies. We sequentially solve the above discretized governing equations corresponding to all basic variables except pressure. To develop the method to solve for pressure, we first tried to develop the continuity equation of solid phase into an equation of pressure correction since the continuity equation of liquid phase has been used to obtain the volume fraction of liquid phase. It was found that this method was not successful because the result was very unstable and unrealistic. This may result from the fact that the driven-phase flow field (solid) at the intermediate stage of the iterative cycle is used to obtain the pressure of the driving-phase flow field (liquid). The effect of enthalpy field at the intermediate stage of the iterative cycle was introduced by the source term of solid phase continuity equation. It should be more reasonable to construct the pressure correction equation based on the mixture continuity equation. This approach not only introduces the effect of the driving-phase flow field to the calculation of the pressure correction, but also prevents the calculation of the source term of phase change based on the velocities and enthalpies before the computational results converge. It, therefore, improves the stability and convergence of numerical results. The mixture continuity equation can be obtained by adding Eqs. (1) and (2):

$$\frac{\partial}{\partial t}[\varepsilon_l\rho_l+\varepsilon_s\rho_s]+\nabla\cdot[\varepsilon_l\rho_l\mathbf{v}_l+\varepsilon_s\rho_s\mathbf{v}_s]=0. \tag{27}$$

The pressure can be written as the guessed pressure or the previous-iterative value p^* plus the pressure correction p':

$$p=p^*+p'. \tag{28}$$

Similarly, velocities can be written as:

$$u_\alpha=u_\alpha^*+u_\alpha',\quad v_\alpha=v_\alpha^*+v_\alpha',\quad w_\alpha=w_\alpha^*+w_\alpha'. \tag{29}$$

We substitute all the velocity components with these expressions and notice that the values of p^*, u_α^*, v_α^*, and w_α^* are the results of previous iterative cycle in the discretized equation of each velocity component. The discretized equation for each velocity correction can be obtained by omitting the terms containing neighboring grid velocities and separating the pressure gradient term from the source term. For example, the correction of liquid phase velocity component in x-direction, $u'_{l,i+1/2}$, is written as

$$u'_{l,i+1/2}=\left(\frac{\varepsilon}{a_u}\right)_{l,i+1/2}(p'_i-p'_{i+1})\Delta y\Delta z \tag{30}$$

In this formula, a_u is the coefficient a in the left side of the discretied x-momentum equation (see the general form, Eq. (25)). The subscript l indicates liquid phase. Therefore, the velocity-correction formula for $u_{l,i+1/2}$ is

$$u_{l,i+1/2}=u^*_{l,i+1/2}+\left(\frac{\varepsilon}{a_u}\right)_{l,i+1/2}(p'_i-p'_{i+1})\Delta y\Delta z \tag{31}$$

The velocity-correction for other velocity components of two phases can be written in a similar form.

Integrating Eq. (27) over the control-volume and utilizing the above-defined velocity-correction, we obtain the following discretized equation for the pressure correction p' after rearrangement:

$$a_p p'_{i,j,k}=a_{p,i+1}p'_{i+1}+a_{p,i-1}p'_{i-1}+a_{p,j+1}p'_{j+1}+a_{p,j-1}p'_{j-1}+a_{p,k+1}p'_{k+1}+a_{p,k-1}p'_{k-1}+b_p, \tag{32}$$

where

$$a_{p,i+1}=\left[\varepsilon_l\rho_l\left(\frac{\varepsilon}{a_u}\right)_l+\varepsilon_s\rho_s\left(\frac{\varepsilon}{a_u}\right)_s\right]_{i+1/2}(\Delta y\Delta z)^2, \tag{33a}$$

$$a_{p,i-1}=\left[\varepsilon_l\rho_l\left(\frac{\varepsilon}{a_u}\right)_l+\varepsilon_s\rho_s\left(\frac{\varepsilon}{a_u}\right)_s\right]_{i-1/2}(\Delta y\Delta z)^2, \tag{33b}$$

$$a_{p,j+1} = \left[\varepsilon_l\rho_l\left(\frac{\varepsilon}{a_v}\right)_l + \varepsilon_s\rho_s\left(\frac{\varepsilon}{a_v}\right)_s\right]_{j+1/2}(\Delta z\Delta x)^2, \quad (33c)$$

$$a_{p,j-1} = \left[\varepsilon_l\rho_l\left(\frac{\varepsilon}{a_v}\right)_l + \varepsilon_s\rho_s\left(\frac{\varepsilon}{a_v}\right)_s\right]_{j-1/2}(\Delta z\Delta x)^2, \quad (33d)$$

$$a_{p,k+1} = \left[\varepsilon_l\rho_l\left(\frac{\varepsilon}{a_w}\right)_l + \varepsilon_s\rho_s\left(\frac{\varepsilon}{a_w}\right)_s\right]_{k+1/2}(\Delta x\Delta y)^2, \quad (33e)$$

$$a_{p,k-1} = \left[\varepsilon_l\rho_l\left(\frac{\varepsilon}{a_w}\right)_l + \varepsilon_s\rho_s\left(\frac{\varepsilon}{a_w}\right)_s\right]_{k-1/2}(\Delta x\Delta y)^2, \quad (33f)$$

$$a_p = a_{p,i+1} + a_{p,i-1} + a_{p,j+1} + a_{p,j-1} + a_{p,k+1} + a_{p,k-1}, \quad (33g)$$

$$\begin{aligned} b_p = {} & [(\varepsilon_l\rho_l + \varepsilon_s\rho_s)^0_{i,j,k} - (\varepsilon_l\rho_l + \varepsilon_s\rho_s)_{i,j,k}]\Delta x\Delta y\Delta z/\Delta t \\ & + [(\varepsilon_l\rho_l u_l^* + \varepsilon_s\rho_s u_s^*)_{i-1/2} - (\varepsilon_l\rho_l u_l^* + \varepsilon_s\rho_s u_s^*)_{i+1/2}]\Delta y\Delta z \\ & + [(\varepsilon_l\rho_l v_l^* + \varepsilon_s\rho_s v_s^*)_{j-1/2} - (\varepsilon_l\rho_l v_l^* + \varepsilon_s\rho_s v_s^*)_{j+1/2}]\Delta z\Delta y \\ & + [(\varepsilon_l\rho_l w_l^* + \varepsilon_s\rho_s w_s^*)_{k-1/2} - (\varepsilon_l\rho_l w_l^* + \varepsilon_s\rho_s w_s^*)_{k+1/2}]\Delta x\Delta y. \end{aligned} \quad (33h)$$

3.3. Solution method

Up to this point, we have formulated all the equations needed to obtain the basic variables. All of the above discretized equations, including that for the pressure correction, have the same algebraic equation form as Eq. (25). We can then develop a special subroutine to solve the general form algebraic equation using the iterative method. The solution process for a different basic variable is different only in calculating the coefficients and the constant term in the discretized equation. When the coefficients and constant term are calculated, the interface values of grid-centered quantities and the grid-centered values of the velocity components are obtained by the interpolation since the staggered grid is used. The harmonic mean is employed for the properties such as densities, effective conductivities and so on. The arithmetic mean is employed for the other quantities. The ADI (alternating-direction implicit) method is used to solve the algebraic equations.

The volume fraction of liquid calculated based on the liquid continuity equation may not agree with the total mass conservation before iterative cycle converges. It may cause the unstableness or divergence of the iterative process. Therefore, we employ the total mass conservation of the entire computational field to obtain the volume fraction correction of liquid in an iterative cycle as follows,

$$\varepsilon_l' = \frac{\sum[(1-\varepsilon_l^*)\rho_s + \dot{m}\Delta t - (1-\varepsilon_l^0)\rho_s^0]\Delta x\Delta y\Delta z}{\sum \rho_s\Delta x\Delta y\Delta z}. \quad (34)$$

From physical phenomena in two-phase flow with water and ice particles as a pair, it is known that the ice particles float upward due to the buoyancy as well as moves downstream due to the inertia and other forces exerted to ice particles by water. The volume fraction of water should be 1 and does not need to be corrected in the area

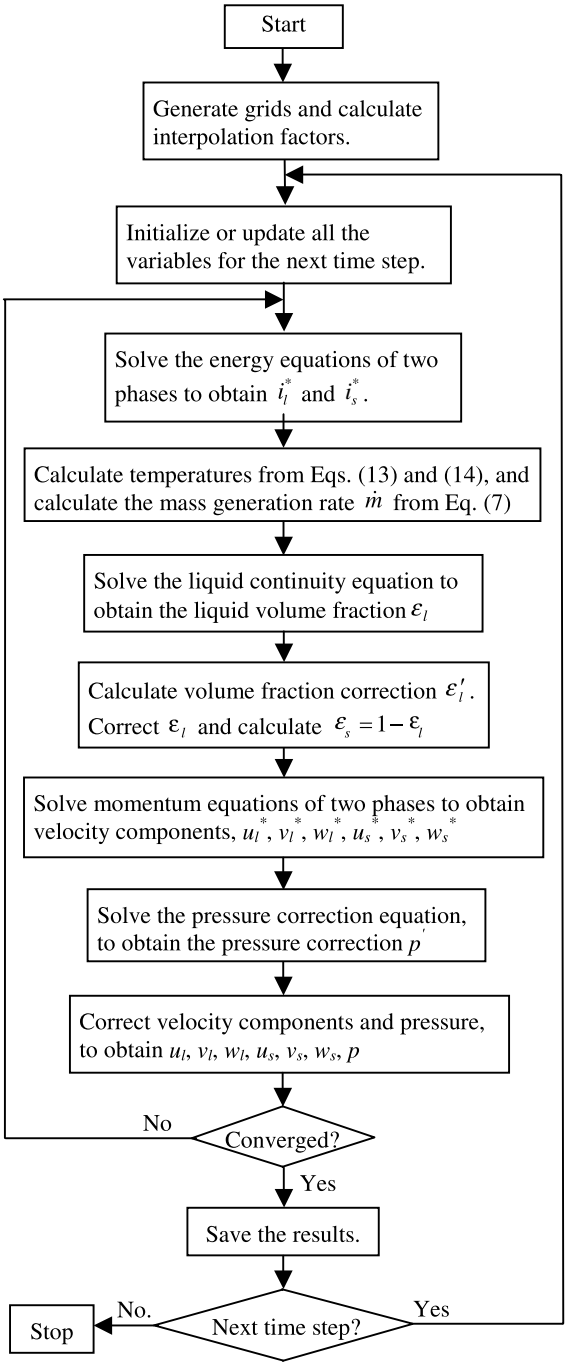

Fig. 2. Flow chart for solving the problem of coupled liquid–solid two-phase flow and heat–mass transfer with phase change in the solid phase.

where there is no ice at the end of last time step. In Eq. (34), therefore, $\sum$ means summation in the region where the ice exists at the end of last time step.

The change in the ice sphere diameter is updated at the end of iterative cycle for each time step. When the iterative cycle has converged and the iterative volume fractions, velocities and temperatures have been established, the diameter distribution of ice sphere in the computational field can be calculated from Eq. (23).

We calculate the equations in the entire computational domain unlike previous studies where the computational domain is divided as two domains, pure liquid domain and liquid–solid domain. Only liquid phase conservation equations were solved in the liquid domain and two-phase conservation equations were solved in the liquid–solid domain in those studies. The present treatment avoids the complexity in the interface conditions as shown in the earlier studies, although it requires additional computational time for solving the solid equations in liquid-only region. When the volume fraction of solid phase equals zero in liquid-only region, the coefficients in Eq. (25) of solid phase variables become zero. Therefore, values of solid phase variables at the grid point can be given directly without the iterative computation. This treatment in the program can save the part of additional computational time for solving solid phase equations in liquid-only region without sacrificing the conservation of mass, momentum and energy in the entire computational domain. The results are considered converged when the relative changes in the variables between two successive iterations are less than $10^{-4}\%$.

Development of the field configurations through time takes place in a sequence of time steps. At each time step Δt the computation is accomplished in such a way as to utilize the results developed in the previous time step (or the initial conditions) for the calculation of new values of all field variables, and to store these in the computer in such a way that they can be processed yet again in the following cycle. Considering the balance between the computing efficiency and accuracy/stability, we choose the typical time steps between 0.001 and 0.01 s, where the small time step corresponds to relatively high velocity (also see the detailed discussion about the results below).

In Fig. 2, we summarize the general procedure of the computer code developed in the present study for the solution of the liquid–solid two-phase flow and heat–mass transfer with the phase change. The computer code is written in FORTRAN. All of equations and parameters are non-dimensionalized before they are solved.

4. Results for water flow through packed ice bed

We present some preliminary results to demonstrate our numerical technique. Although in this study we focus on the convective melting of ice particles in hori-

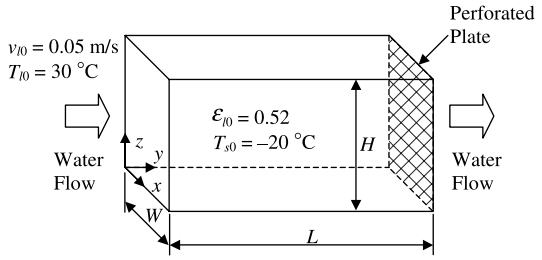

Fig. 3. Computational domain with specified boundary and initial conditions.

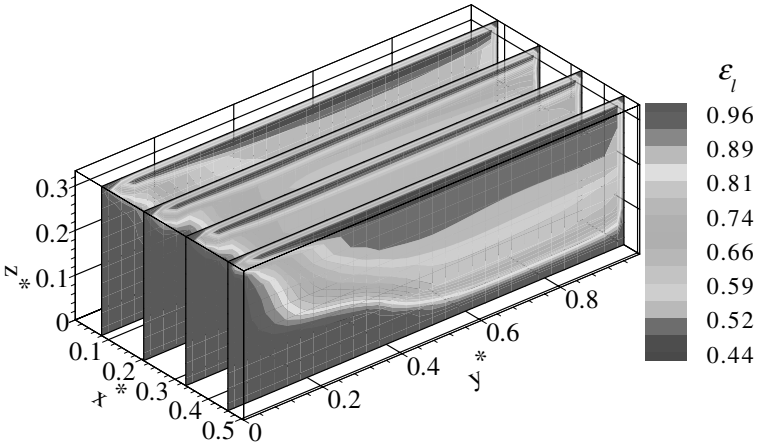

Fig. 4. Volume fraction of water at $t = 24.1$ s and $x/L = 0.0792$, 0.206, 0.333, and 0.459: $v_{l0} = 0.05$ m/s, $T_{l0} = 30$ °C, $\varepsilon_{s0} = 0.52$, $T_{s0} = -20$ °C.

zontally flowing water, the present technique can also be used to simulate the melting process of granular packed bed of other phase-change material in a fluid flow. The reason why we use water and ice particles as liquid and solid phases is mainly that the results can be validated by the experimental results in [1]. As illustrated in Fig. 3, the computational region is an open channel section with a rectangular cross-section. Initially, the full amount of ice particles with the packed volume equal to the computational domain at a given initial temperature is suddenly placed in the horizontally flowing water, which is assumed fully developed initially in the test section. The packed bed forms during convective melting as a result of gravity and horizontal flow with a downstream perforated plate that stops melting particles [1].

4.1. Initial and boundary conditions

The initial volume fraction of the particles is assumed uniform. For the momentum equations, the domain is surrounded by three impermeable, no-slip rigid walls for both phases (two vertical walls at sides and one bottom wall) and by a wall at the exit, which is permeable for the water and impermeable (no-slip rigid) for the ice phase. The top boundary condition is a free surface for both phases. At the entrance, the influx of water with a uniform velocity is prescribed. For the thermal energy equations, the bottom wall, top surface, and sidewalls are considered as adiabatic surfaces for both phases. At the entrance, the inlet temperature of water is assumed uniform. At the exit, the continuity energy outflow boundary conditions are assumed for both phases.

In order to compare numerical results with experimental results, computations were carried out for a typical experimental case presented in Part I of this study [1]. In this case, the width, height and length of the computational region are 152, 100, and 300 mm, respectively. Water flows at the entrance with the constant velocity of 0.05 m/s and the constant temperature of 30 °C. The initial temperature of ice particles is −20 °C and the initial equivalent spherical diameter of 26.2 mm. The initial volume fraction of water in the section is uniformly distributed at 0.52. The grid number adopted in the preliminary computation is 34 in the x-direction, 62 in the y-direction, and 22 in the z-direction, for a total of 46,376. A fixed time step of $\Delta t = 0.005$ s was used. The computation used about 285.66 h of computational time on a Sun Blade 1000 workstation with two 750 MHz UltraSPARC III processors and 1 GB memory.

4.2. Liquid volume fraction

Fig. 4 shows the distribution of water volume fraction at $t = 24.1$ s. The melting ice particles float to the upper field since the density of ice is less than that of water under the gravity condition, and are pushed towards downstream. In the figure, the value of the water volume fraction is very close to unit in the entrance region (left-lower region). If we defined a value of water volume fraction, such as 0.97, at which the interface between the packed ice particles and liquid water is present, the entire domain can be divided as the packed bed of ice particles region in the upper and downstream portions of the domain and the liquid-only region in the lower and upstream portions. Fig. 5 shows the typical interfaces at the three time points in the convective

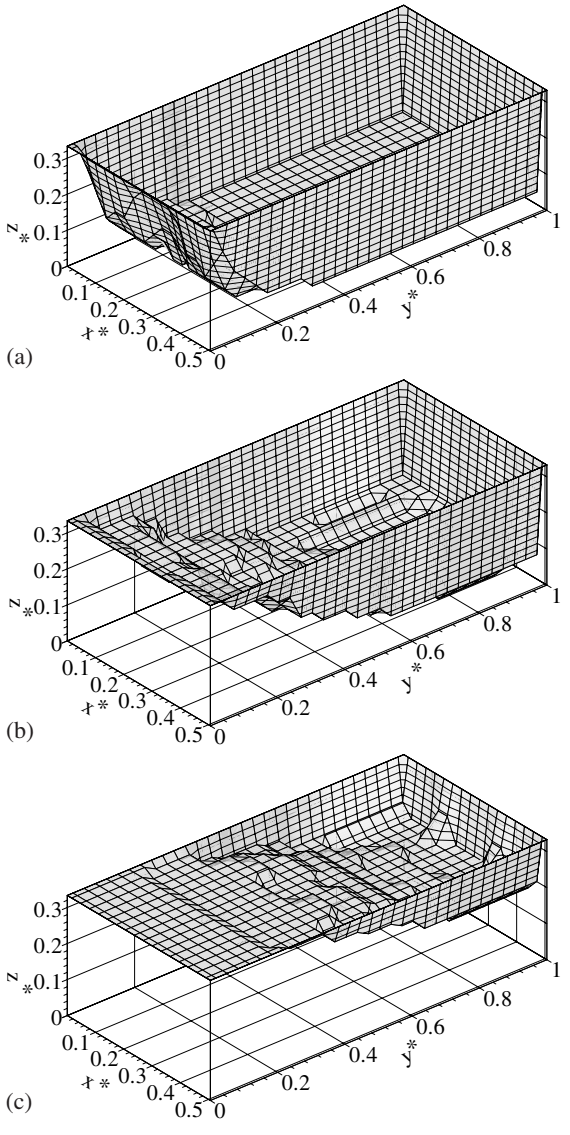

Fig. 5. Interface between the water domain and the water–ice domain in the convective melting process: (a) $t = 13.7$ s; (b) $t = 37.9$ s; (c) $t = 76.6$ s: $v_{l0} = 0.05$ m/s, $T_{l0} = 30$ °C, $\varepsilon_{s0} = 0.52$, $T_{s0} = -20$ °C.

melting process. The interface clearly shows the variation of the packed bed thickness as convective melting of the ice particles in the packed bed continues. The calculated packing pattern of the ice particles in this horizontal flow agree qualitatively well with the experimental observations presented in Part I [1].

4.3. Velocity and temperature distributions

Fig. 6(a) shows the spatial distribution of the liquid phase velocity vectors along with the liquid volume fraction distribution. At that particular time, the liquid near the entrance region flows downwards gradually because of the flow resistance from the packed bed in the upper region. As flowing further downstream, water moves up gradually because the passage for water becomes narrower in the lower region due to the thick packed bed. In the bottom half of the domain towards downstream a parallel flow pattern exists except near the vertical side walls where a downward flow is observed due to the flow mixing with the cold melt discharge. Because the ice particles tend to pack in upper region,

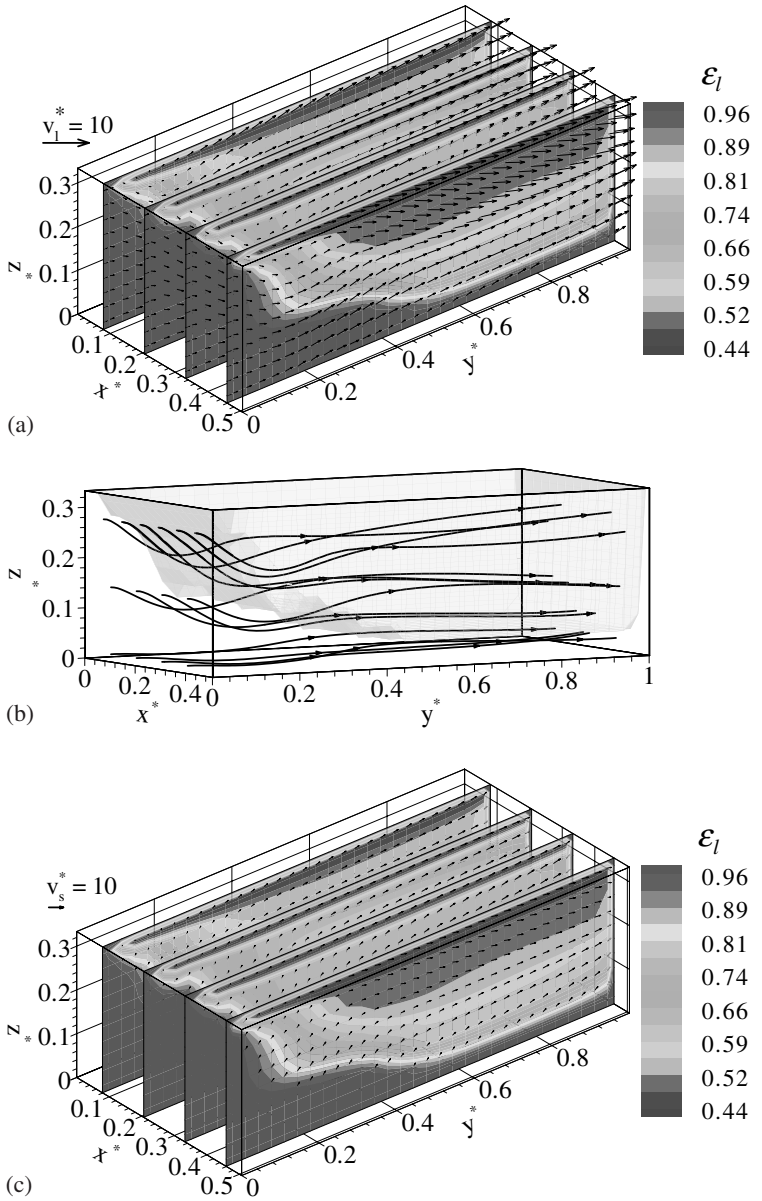

Fig. 6. (a) Velocity vectors of water, (b) streamlines of water flow and interface of packed bed, and (c) velocity vectors of solid phase at $t = 24.1$ s and $x/L = 0.0792$, 0.206, 0.333, and 0.459: $v_{l0} = 0.05$ m/s, $T_{l0} = 30$ °C, $\varepsilon_{s0} = 0.52$, $T_{s0} = -20$ °C.

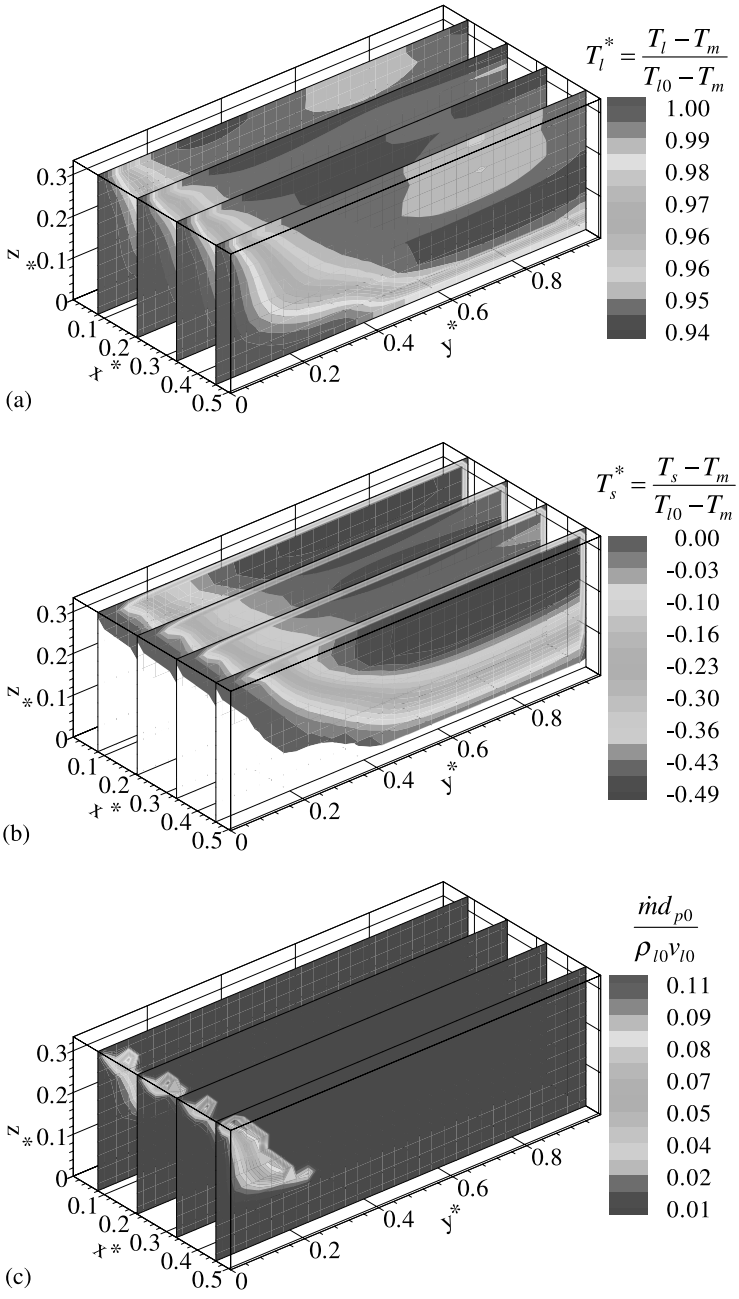

Fig. 7. (a) Temperature distribution of water flow, (b) temperature distribution of solid phase, and (c) melting rate of solid phase at $t = 24.1$ s and $x/L = 0.0792$, 0.206, 0.333, and 0.459: $v_{l0} = 0.05$ m/s, $T_{l0} = 30$ °C, $\varepsilon_{s0} = 0.52$, $T_{s0} = -20$ °C.

the volume fraction of ice increases, which causes the cross-sectional area for water passage to decrease in the packed bed region. Since water is incompressible, the velocities of water in the upper region are greater than in the lower region, as shown in Fig. 6(a). The flow characteristics are also clearly illustrated by the streamlines in Fig. 6(b).

In Fig. 6(c), the spatial distribution of the solid phase velocity vectors is shown overlaying on the liquid volume fraction distribution for the same condition as in

Fig. 6(a). The motion of solid phase is driven by the water flow. Therefore, the velocity vector of solid tends to follow that of liquid in the packed bed. There are no particles near the entrance region so that no velocity vector appears there. The velocity vector approaches zero at the exit because that the perforated plate stops the particles.

The temperature distribution of water along the flow direction can be seen in Fig. 7(a). The temperature of water decreases gradually towards the downstream with the low temperature region primarily inside the packed bed, which is also corresponding to the lowest liquid volume fractions. Fig. 7(b) shows the temperature distribution of solid phase. The ice particles pack in the upper and downstream portions. The water with higher temperature flows against the packed bed. At that particular time ($t = 24.1$ s), the ice particles are being heated near the interface. A relatively sharp temperature gradient near the bed interface indicates a melting zone that is kept at the phase-change temperature, while the temperature inside of packed bed is still below the phase-change temperature. The distribution of local melting rate of the solid phase, shown in Fig. 7(c), clearly supports that observation. This phenomenon is partly because the initial solid phase temperature is low (about −20 °C). For an initially warm ice pack (e.g., −5 °C), the melting zone has been found to be much wider (results are not shown here). It should be noted from Figs. 4–7 that the simulation results are approximately symmetrical about the vertical center plane, but clearly shows the influence of the vertical side walls on the non-uniform distribution of all the variables in the x^*-direction.

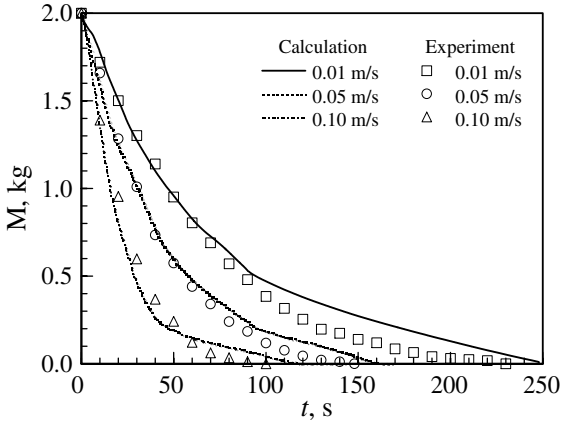

Fig. 8. Comparison of the calculated results (the present study) and experimental results [1] on the variation of mass of packed bed with time under different water velocities at inlet: $T_{l0} = 30$ °C, $\varepsilon_{s0} = 0.52$, $T_{s0} = -20$ °C, $M_{s0} = 2$ kg.

4.4. Comparison with experimental results

In Fig. 8, the calculated mass of ice particles in the packed beds from the numerical model is compared with the measured one. Three experimental cases are presented using the results in Part I [1]. They are under different water velocity conditions, $v_{l0} = 0.01$, 0.05, and 0.10 m/s, respectively. The comparison shows that the predicted mass variations with time agree well with the experimental results, especially in the first period of melting process. The main reason for the shown discrepancy is that the correlation for

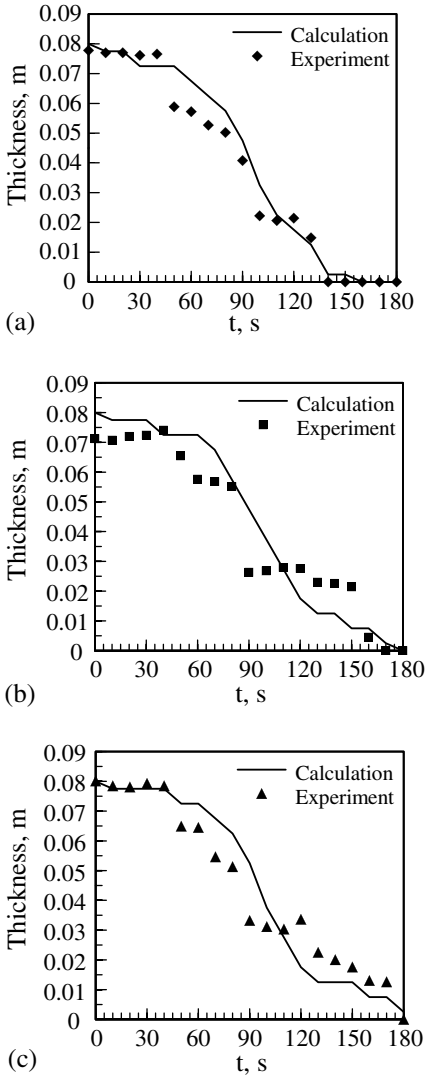

Fig. 9. The comparison of bed thickness between the numerical results and the experimental data: (a) $y = 0.15$ m; (b) $y = 0.24$ m; (c) $y = 0.33$ m.

the heat transfer coefficient between fluid and particles, Eq. (22), was developed for the large size particle without melting. The uncertainty would increases with the decrease in the particle size during the late period of melting process. The melting process also strongly affects the heat transfer characteristics between the fluid and particle [15,16]. There has been a lack of the correlation for the local heat transfer coefficient between fluid and particles with melting covering the entire melting period.

The comparison between the numerically calculated and measured packed bed thickness is shown in Fig. 9. The experimental bed thickness is obtained by measuring the vertical distance from the free surface to the interface according to the visual observation from the side view. Accordingly, we obtained the thickness by calculating the vertical distance from the free surface to the bottom bed interface. This way, we determine the highest value of the thickness in the x-direction to compare the measurement data. The results shown in Fig. 9 indicate that the numerical results agree reasonably well with the experimental results.

4.5. Grid-independence exercise

To examine the dependence of the solution on the grid parameters, computations were performed with other two different grid numbers of $68 \times 122 \times 42$ in x-, y-, and z-directions, respectively, and $18 \times 32 \times 12$ in x-, y-, and z-directions. The time step remains at $\Delta t = 0.001$ s. The results show that the difference of results on grid number of $68 \times 122 \times 42$ and $34 \times 62 \times 22$ is negligible. Therefore, the grid-independent result can be obtained when the grid numbers are more than $34 \times 62 \times 22$ in the present study.

5. Conclusions

A numerical model is developed, based on the theory of interacting continua, to simulate the complex liquid–solid two-phase flow for a melting packed bed subject to a horizontal force convection. The model is solved using the SIMPLE method, for which the pressure correction method is developed using the two-phase mixture continuity equation. The method features the global solutions for conservation equations including both the liquid–solid region and the liquid-only region. This is to ensure the global conservation of mass, momentum and energy of two phases. The motion and volume fraction of solid phase during melting process are predicted in addition to the usual prediction of fluid flow field and phase temperatures. No assumptions of motionless solid particles and the constant porosity or the constant volume are used.

The numerical code developed in the present study has proved to be grid-independent. The computational results reveal the detail of the flow and melting characteristics in the melting packed bed. The validation of the model through a case study by experimental results indicates that the model achieves a reasonably good accuracy in simulating both the melting process and the packing pattern of the granular packed bed. It has been pointed out that the constitutive equation for the local heat transfer coefficient is a crucial factor influencing the accuracy of the model. This study lays a foundation for comprehensive, parametric study of various coupling physical effects in convective melting of solid particles. It can be extended to study both packed and dispersed particles.

Acknowledgements

The supports from NASA (Grant No. NAG3-1797) and NSF (Grant No. 97206268) are greatly appreciated. The authors thank Mr. Natarajan Chandrasekaran for providing the assistance in data analysis.

References

[1] Y.L. Hao, Y.-X. Tao, Non-thermal equilibrium melting of granular packed bed in horizontal forced convection. Part I: experiment, Int. J. Heat Mass Transfer, in press.
[2] D.A. Kearns, G.A. Plumb, Direct contact melting of a packed bed, ASME J. Heat Transfer 117 (2) (1995) 452–457.
[3] G.A. Plumb, Convective melting of packed beds, Int. J. Heat Mass Transfer 37 (5) (1994) 829–836.
[4] J. Pak, O.A. Plumb, Melting in a two-component packed bed, J. Heat Transfer 119 (3) (1997) 553–559.
[5] A.S. Sabau, Y.-X. Tao, On mathematical modeling of convective melting of a granular porous medium, in: K. Goodson et al. (Eds.), ASME Proceedings of the32nd National Heat Transfer Conference, Baltimore, MD, HTD-Vol. 349, 1997, pp. 197–204.
[6] J. Jiang, J. Sun, V. Ganesan, Y.-X. Tao, Numerical modeling of two-dimensional convective melting of granular packed beds, in: K.J. Michael, M. Di Marzo (Eds.), ASME Proceedings of the 33rd National Heat Transfer Conference, Albuquerque, NM, NHTC99-216, 1999.
[7] S.V. Patankar, Numerical Heat Transfer and Fluid Flow, Hemisphere Publishing Corporation, New York, 1980.
[8] J.A. Boure, J.M. Delhaye, General equations and two-phase flow modeling, in: H. Gad (Ed.), Handbook of Multiphase Systems, Hemisphere Publishing Corporation, New York, 1982, pp. 1.36–1.95.
[9] D. Gidaspow, Hydrodynamics of fluidization and heat transfer: supercomputer modeling, Appl. Mech. Rev. 39 (1) (1986) 1–23.
[10] P.N. Rowe, Drag forces in a hydraulic model of a fluidized bed, Trans. Inst. Chem. Eng. 39 (1961) 175–180.

[11] R. Jackson, Fluid mechanical theory, in: J. Davidson, F. Harrison (Eds.), Fluidization, Academic, London, 1971, pp. 63–119.
[12] J.X. Bouillard, R.W. Lyczkowski, D. Gidaspow, Porosity distributions in a fluidized bed with an immersed obstacle, AIChE J. 35 (6) (1989) 908–922.
[13] R. Bauer, E.U. Schlumder, Effective radial thermal conductivity of packing in gas flow, Int. Chem. Eng. 18 (1978) 189–204.
[14] N. Wakao, S. Kaguei, Heat and Mass Transfer in Packed Beds, Gordon and Breach, New York, 1982.
[15] Y.L. Hao, Y.-X. Tao, Melting of a solid sphere under forced and mixed convection: flow characteristics, J. Heat Transfer 123 (5) (2001) 937–950.
[16] Y.L. Hao, Y.-X. Tao, Heat transfer characteristics of melting ice spheres under forced and mixed convection, J. Heat Transfer 124 (5) (2002) 891–903.